Geophysical Monitoring of Coupled Microbial and Geochemical Processes During Stimulated Subsurface Bioremediation

KENNETH H. WILLIAMS,*,†
ANDREAS KEMNA,‡
MICHAEL J. WILKINS,§
JENNIFER DRUHAN,‖ EVAN ARNTZEN,⊥
A. LUCIE N'GUESSAN,⊥
PHILIP E. LONG,⊥ SUSAN S. HUBBARD,†
AND JILLIAN F. BANFIELD§,‖

Lawrence Berkeley National Laboratory, Berkeley, California 94720, Department of Geodynamics and Geophysics, University of Bonn, 53115 Bonn, Germany, Department of Environmental Science, Policy and Management, University of California, Berkeley, California 94720, Department of Earth and Planetary Science, University of California, Berkeley, California 94720, and Pacific Northwest National Laboratory, Richland, Washington 99352

Understanding how microorganisms alter their physical and chemical environment during bioremediation is hindered by our inability to resolve subsurface microbial activity with high spatial resolution. Here we demonstrate the use of a minimally invasive geophysical technique to monitor stimulated microbial activity during acetate amendment in an aquifer near Rifle, Colorado. During electrical induced polarization (IP) measurements, spatiotemporal variations in the phase response between imposed electric current and the resultant electric field correlated with changes in groundwater geochemistry accompanying stimulated iron and sulfate reduction and sulfide mineral precipitation. The magnitude of the phase response varied with measurement frequency (0.125 and 1 Hz) and was dependent upon the dominant metabolic process. The spectral effect was corroborated using a biostimulated column experiment containing Rifle sediments and groundwater. Fluids and sediments recovered from regions exhibiting an anomalous phase response were enriched in Fe(II), dissolved sulfide, and cell-associated FeS nanoparticles. The accumulation of mineral precipitates and electroactive ions altered the ability of pore fluids to conduct electrical charge, accounting for the anomalous IP response and revealing the usefulness of multifrequency IP measurements for monitoring mineralogical and geochemical changes accompanying stimulated subsurface bioremediation.

* Corresponding author phone: 510.701.1089; e-mail: khwilliams@lbl.gov.
† Lawrence Berkeley National Laboratory.
‡ University of Bonn.
§ Department of Environmental Science, Policy and Management, University of California.
‖ Department of Earth and Planetary Science, University of California.
⊥ Pacific Northwest National Laboratory.

Introduction

Groundwater contamination by industrial sources and nuclear weapons programs has promoted research into the ability of microorganisms to facilitate remediation through the sequestration of aqueous metals and radionuclides in insoluble precipitates (*1*). Much of the research has focused on microorganisms capable of either iron or sulfate reduction, and both classes have been shown to reductively immobilize such contaminants under field conditions (*2, 3*). Given the range of geochemical interactions accompanying biostimulation, the development of monitoring approaches sensitive to both the distribution of subsurface metabolic processes and the precipitation of mineralized end products is sorely needed.

Near surface geophysical techniques represent such an approach, providing information about subsurface environments not directly accessed by boreholes (*4*). An increasing number of studies have utilized electrical geophysical methods to delineate variations in the physical and chemical properties of sediments during biological experiments (*5–8*). Among these methods, the induced polarization (IP) technique has shown excellent sensitivity to enhanced microbial activity (*5, 7, 9–12*). Such studies, combined with theoretical investigations exploring the electrochemical mechanisms underlying the IP response (*13, 14*), suggest it is well suited to monitoring stimulated subsurface bioremediation under field conditions.

Analogous to laboratory electrochemical approaches, the IP method involves injection of variable frequency currents into the ground and the measurement of resulting voltage potentials via electrodes located above and below the ground surface. Variations in the phase and magnitude of the applied and measured potentials determine the frequency-dependent electrical properties of the subsurface. Regions exhibiting large phase shifts between the applied and measured potential are found to correspond to regions where charge transfer through the pore fluid is impeded due to a variety of interfacial conduction mechanisms (*15–17*). These include regions where charge transfer changes from electrolytic to electronic (such as in pore-blocking mineralized rocks) or where grain surface features impede the normal flow of current carrying ions (such as in areas of high surface charge density).

In the current study, we investigated whether changes in electroactive ion composition and mineral precipitation accompanying microbial metabolism were detectable using spectral IP monitoring approaches. Additionally, we investigated whether the method could delineate regions of stimulated iron and sulfate reduction due to the accumulation of distinctive electroactive ions (e.g., Fe(II) and dissolved sulfide) and the precipitation of semiconductive minerals, a process known to generate anomalous IP signatures in the laboratory (*11, 12, 18, 19*). The contribution of planktonic and mineral-affixed cells to the spectral IP signatures was not specifically investigated in this study; however, their role in generating measurable IP anomalies in the laboratory has been demonstrated (*7, 9, 10*). As a wide range of IP-generating mechanisms may accompany field biostimulation activities, the unambiguous discrimination of any one mechanism may be particularly challenging.

The contribution of electroactive ions to anomalous IP signals results from their ability to participate in heterogeneous electron transfer reactions with redox active minerals (*20, 21*). In contrast to the majority of ions in groundwater (e.g., Na^+, Ca^{2+}, Cl^-, and SO_4^{2-}), Fe(II) and sulfide engage in
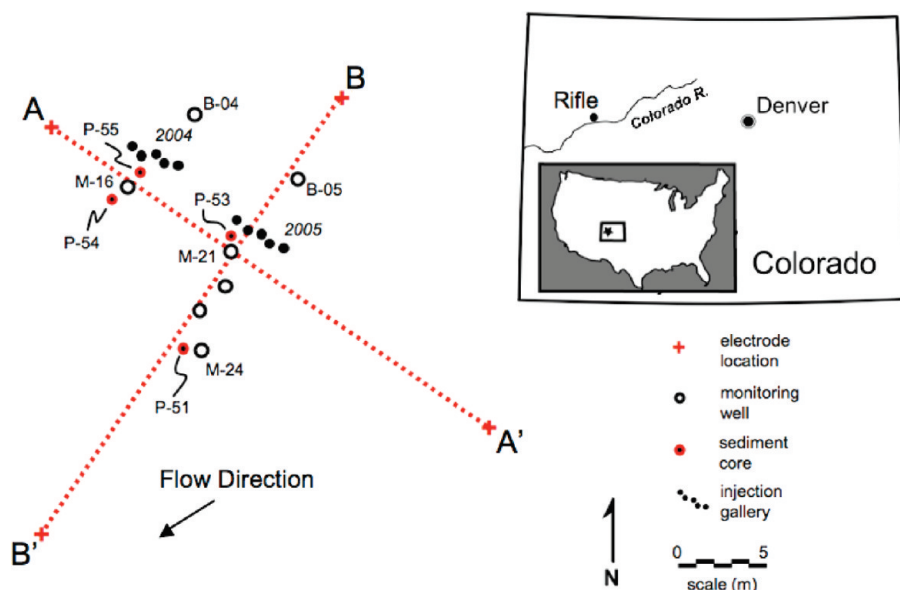
FIGURE 1. Plan map of the injection and monitoring well locations at the Rifle, CO field site; groundwater flow direction is indicated. Surface induced polarization (IP) geophysical data were acquired along two transects oriented perpendicular (A—A') and parallel (B—B') to groundwater flow.

charge transfer reactions with a variety of minerals (22–24), with the resistance to charge transfer decreasing as the concentration of electroactive ions increases (21). This may occur even in the absence of newly formed mineral phases, given the presence of naturally occurring authigenic semi-conductive minerals. The rate at which charge transfer occurs is influenced by a variety of factors, including the composition and concentration of electroactive ions, as well as the reactive surface area of the mineral enabling the charge transfer reaction (21). As a result, the time scale over which charge transfer occurs will depend upon the specific electrochemical and mineralogical conditions, yielding a unique frequency-dependent response.

Although critical frequencies may vary depending upon whether measurements are made in the laboratory or the field due to scaling effects, we propose that IP measurements made at higher frequencies (e.g., >10 Hz) should be more sensitive to geochemical conditions that facilitate the rapid transfer of electrons across mineral interfaces; measurements made at lower frequencies should theoretically track more sluggish electrochemical processes. Rapid electron self-exchange rates between aqueous Fe(III) and Fe(II) (25) suggest that Fe(II)-mediated charge transfer processes should dominate at higher measurement frequencies, with larger phase shifts theoretically diagnostic of iron reduction. Conversely, kinetically slower electron transfer processes mediated by the oxidation of aqueous sulfide (26, 27) should dominate at lower frequencies and be diagnostic of sulfate reduction. Where both processes are stimulated, the precipitation of FeS and the persistence of either Fe(II) or sulfide in the pore space should lead to an increase in the phase response over a wide range of frequencies, with a frequency-dependent behavior governed by the predominant electroactive ion and the precipitate surface area and grain size (13, 28, 29).

Materials and Methods

Site Description. A comprehensive description of the Rifle Integrated Field Research Challenge (IFRC) site has been presented elsewhere (2, 30). Briefly, the site is located on a flood plain in Northwestern Colorado (Figure 1), and the local aquifer is comprised of ca. 6.5 m of unconsolidated sands, silts, clays, and gravels. The dominant iron bearing minerals consist of goethite, chlorite, magnetite, and he-

matite. The average depth to groundwater is 3.5 m below ground surface (bgs), and the flow direction is toward the southwest. Values for hydraulic conductivity and pore water velocity range from 2–30 m/d and 0.3–0.5 m/d, respectively. Background geochemical conditions consist of low dissolved oxygen (<16 μM), circumneutral pH, elevated specific conductivity (2400 μS/cm), and sulfate (7–9 mM) and Fe(II) (4–45 μM) concentrations that vary spatially.

Groundwater Amendment and Sampling. Groundwater was pumped from an upgradient portion of the aquifer into a storage tank and amended with sodium acetate and bromide to achieve aquifer concentrations of 10 and 1 mM, respectively. Injection in the gallery (Figure 1) labeled "2005" involved a 68-day acetate amendment targeting sulfate reduction, whereas the gallery labeled "2004" was used for a 21-day amendment targeting iron reduction; acetate injection was halted on the same date in both galleries.

Groundwater samples were pumped at 2–5 day intervals from amended and unamended wells (Figure 1), and Fe(II) and dissolved sulfide concentrations of filtered samples (0.2 μm) were determined colorimetrically (31, 32). Filtered samples (0.1 μm) were obtained from well M-21 for scanning and transmission electron microscopy (SEM and TEM) analysis and preserved anaerobically until the time of analysis (11).

Sediment Sampling and Analysis. Sediment cores were recovered from multiple locations 59 days after beginning acetate injection in the 2005 gallery (e.g., P-51; Figure 1). Samples from each core were collected and dried anaerobically and analyzed for both acid volatile sulfide (AVS) and Fe(II)/Fe(III) content, as described elsewhere (30).

IP Data Collection and Analysis. Surface IP data were acquired along two 30 m transects: one parallel (A—A') and one perpendicular (B—B') to groundwater flow direction (Figure 1). Data were acquired using a modified dipole–dipole configuration between 30 equally spaced Cu/CuSO$_4$ electrodes, with a dipole spacing of 4 m and a total of 27 potential dipoles per current dipole. Contact resistance between the electrodes ranged from 400–800 Ω. All data sets consisted of reciprocal data pairs, wherein electrodes used to apply current and measure voltage were reversed and data reacquired. Data were collected using a Zonge GDP-32 at three frequencies (0.125, 1, and 10 Hz) with a Zonge ZT-30 transmitter (55 V; maximum current density of 3 mA/cm^2).
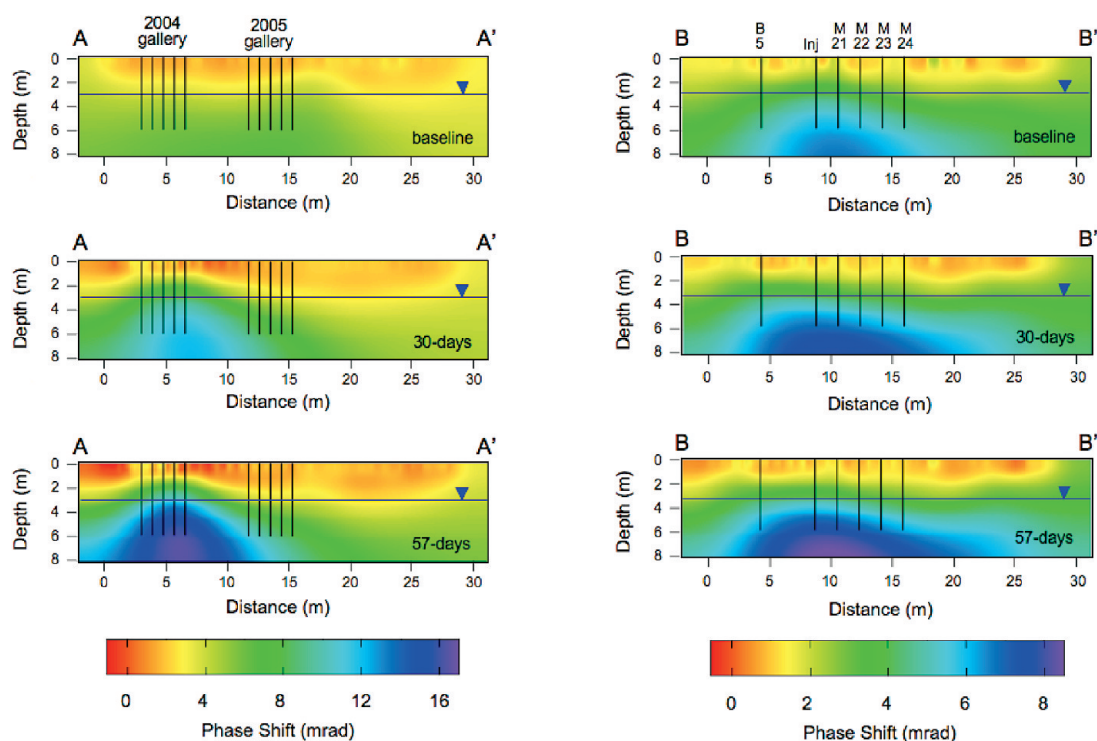
FIGURE 2. Phase inversion results for the surface IP data (0.125 Hz) acquired at three time intervals along A—A′ and B—B′; their locations and those of the indicated boreholes are shown in Figure 1.

The associated relative and absolute resistivity errors were 1% and 0.0001, respectively. Poor data reciprocity between a majority of dipoles prevented use of the 10 Hz data. Repeated acquisition of baseline data prior to acetate injection assessed data reproducibility in the absence of biostimulation. Subsequent data were acquired 30 and 57 days after injection began in the 2005 gallery, with the latter data set collected 14 days after starting injection in the 2004 gallery.

The IP inversion results were obtained using CRTomo, which utilizes an algorithm that solves directly for conductivity magnitude and phase by consequent adoption of complex calculus, with the region of interest represented as a two-dimensional distribution of magnitude and phase values (33). The two-dimensional approach to processing represents a legitimate approximation for the study site where vertical rather than lateral conductivity variations predominate. Although electromagnetic induction effects can dominate the IP spectrum above 10 Hz (34), accounting for such effects was neglected, given the data reported (≤10 Hz).

Laboratory Column Experiment. The sensitivity of the IP method to the products of iron and sulfate reduction was examined in laboratory columns using aquifer materials perfused with acetate-amended (5 mM) site groundwater for 90 days, and a flow rate of 0.30 m/d. Effluent and midcolumn concentrations of aqueous $Fe(II)$ and sulfide were quantified as described above. Electrical measurements of phase and conductivity magnitude were made at regular intervals using a two-channel dynamic signal analyzer over the frequency range 1—1000 Hz (12).

Results

Impact of Biostimulation on Field IP Signals. The baseline electrical properties of the aquifer reveal a resistivity and phase structure comprised of three distinct layers and moderate lateral variations (Supporting Information (SI) Figures S1 and S2). The raw baseline and differential IP data are plotted as pseudosections in SI Figures S3 and S4, respectively. In the absence of biostimulation, the phase change was less than ±1% (SI Figure S4). Similarly reproducible values for electrical resistivity were observed over the same interval (data not shown).

During acetate injection, the phase response of the sediments increased significantly above their baseline values (Figure 2). The phase anomalies occurred beneath the water table and were generally confined to locations downgradient of the injection galleries. Transect A—A′ exhibited the greatest temporal phase increases and is the focus of the results presented below. Phase shifts exceeding 16 mrad at 0.125 Hz were observed after 57 days, an increase of more than 125% above baseline. In contrast, the electrical resistivity of the sediments increased only slightly with time (SI Figure S5).

Differences in the magnitude of the phase response at 1 and 0.125 Hz were observed during the two postamendment measurement periods (Figures 3 and SI Figure S6). Phase increases were greater at 0.125 Hz prior to starting acetate injection in the 2004 gallery, after which time, the trend was reversed. Data collected at 1 Hz exhibited a greater differential phase response, increasing by 10—12 mrad above preinjection values, while that collected at 0.125 Hz increased by 6—8 mrad over the same time interval. In both instances and regardless of frequency, the phase anomalies were offset from locations immediately downgradient from the 2005 injection gallery.

The temporal IP results along transect A-A′ generally replicated those observed the previous year during a 30-day acetate injection in the 2005 gallery (SI Figure S7). The largest change in the phase response was similarly offset from the injection wells in the direction of the 2004 gallery; however, acetate was not injected into the 2004 gallery at any point during data collection.

Impact of Acetate Injection on Aquifer Geochemistry and Mineralogy. Following injection in the 2005 gallery, acetate and bromide (data not shown) were detected in M-21 within 3 days. The concentration of $Fe(II)$ rose rapidly within 7 days, followed by large increases in dissolved sulfide after day 15 (Figure 4). During the initial accumulation of sulfide, $Fe(II)$ concentrations fell to levels below detection. The
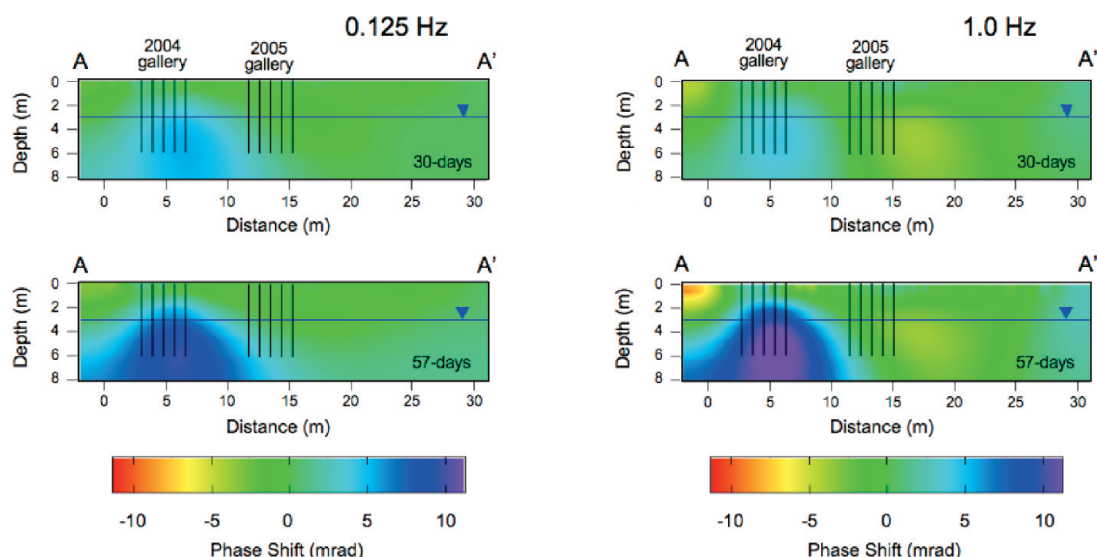
FIGURE 3. Differential surface IP phase inversion results acquired along A—A′ at 0.125 and 1 Hz. The results were obtained by subtracting data obtained after 30 and 57 days from the baseline data.
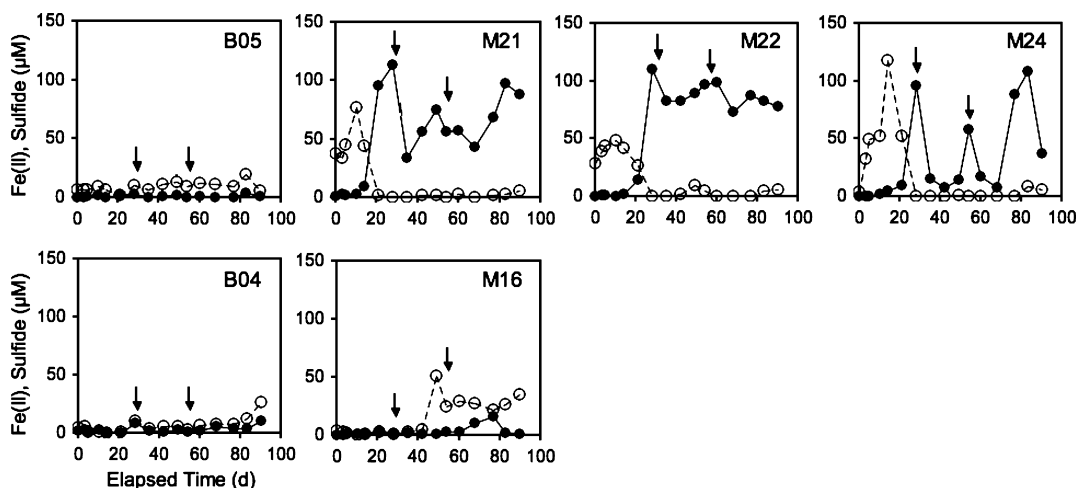

FIGURE 4. Changes in Fe(II) (○) and sulfide (●) concentrations accompanying acetate injection; groundwater flow is from left to right. Acetate injection in the 2005 and 2004 galleries began on day 0 and day 43, respectively, and the induced polarization measurements were made at the times indicated (arrows).

appearance of dark precipitates on both tubing and syringe filters followed the initial accumulation of sulfide.

Subsequent to acetate injection in the 2004 gallery, downgradient concentrations of Fe(II) in M-16 increased abruptly (Figure 4). Although low levels of dissolved sulfide were detected, the concentration of Fe(II) remained elevated throughout the period of acetate amendment. At no point were dark precipitates observed during the sampling of wells downgradient of the 2004 gallery.

Postinjection sediment samples revealed spatially distinct distributions of AVS and Fe(II). Sediments obtained from regions downgradient of the 2005 injection gallery contained elevated levels of AVS, ranging from $0.4-1.28\ \mu$mol/g at P-51 to $1.0-1.74\ \mu$mol/g at P-53, and were visibly darkened (SI Figure S8). Sediments obtained from locations downgradient of the 2004 gallery had AVS values similar to background sediments, ranging from $0-0.06\ \mu$mol/g at P-54 and P-55. The Fe(II)/Fe(total) ratios ranged from $0.5-0.68$ for all biostimulated locations, as compared to background sediments, which ranged from $0.1-0.14$.

SEM and TEM analysis of dark precipitates obtained from M-21 revealed abundant cells and associated minerals (Figure 5). Energy dispersive X-ray analysis confirmed the precipitates to be composed primarily of iron and sulfur, although the presence of calcium and carbon suggest calcite was also present. TEM analysis confirmed the association of the mineral precipitates with cellular membranes (SI Figure S9). The precipitates ranged in size from individual $2-4$ nm nanocrystals to $100-150$ nm aggregates.

Laboratory IP Response Accompanying Iron and Sulfate Reduction. The temporal laboratory IP data corroborated the field measurements, and the baseline phase response was consistent with the presence of clay minerals and semiconductive iron oxides, such as magnetite and hematite. For frequencies >10 Hz, the baseline laboratory phase response (SI Figure S10) was in close agreement with the baseline field values (SI Figure S6). The phase values increased within 5 days, tracking the onset of iron reduction as evidenced by the accumulation of Fe(II) (Figure 6A). As the sediments began to darken, Fe(II) steadily decreased and phase values increased across the entire frequency range, before stabilizing or decreasing slightly as Fe(II) concentrations fell below 10 μM. As sulfide levels increased above 100 μM on day 45, Fe(II) was no longer detected and dark precipitates occupied much of the visible pore space. The significant increase in sulfide concentration over the remaining 45 days was accompanying by a steady increase in the phase response across all but the highest frequencies.
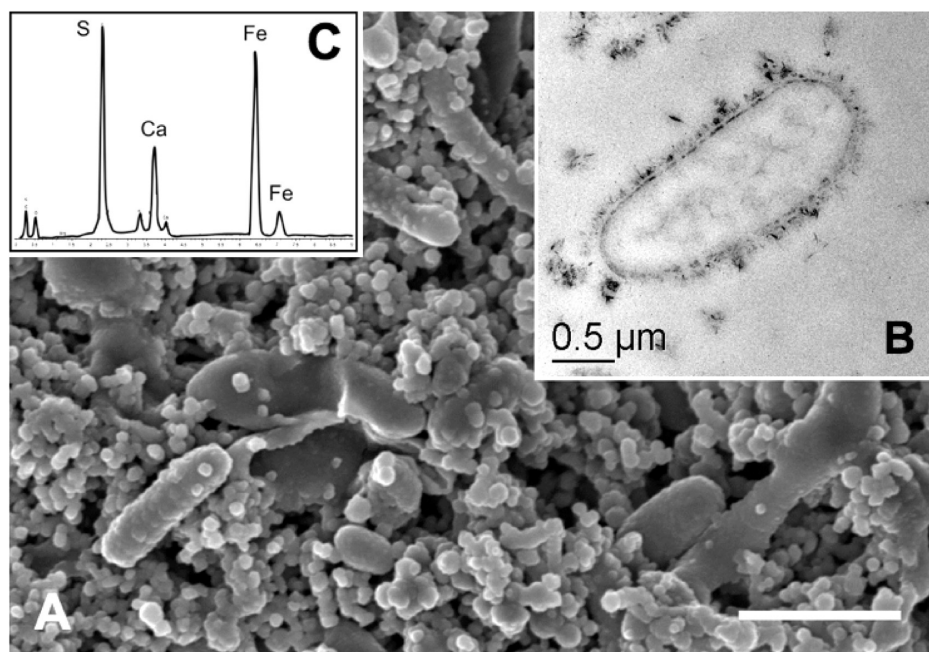
FIGURE 5. (A) SEM image of filter (0.1 μm) residue obtained from groundwater pumped from well M-21 on day 60. Bar: 2 μm. (B) High-resolution TEM image of individual cell and surface-associated precipitates. (C) Energy dispersive X-ray spectrum of precipitates in (A).
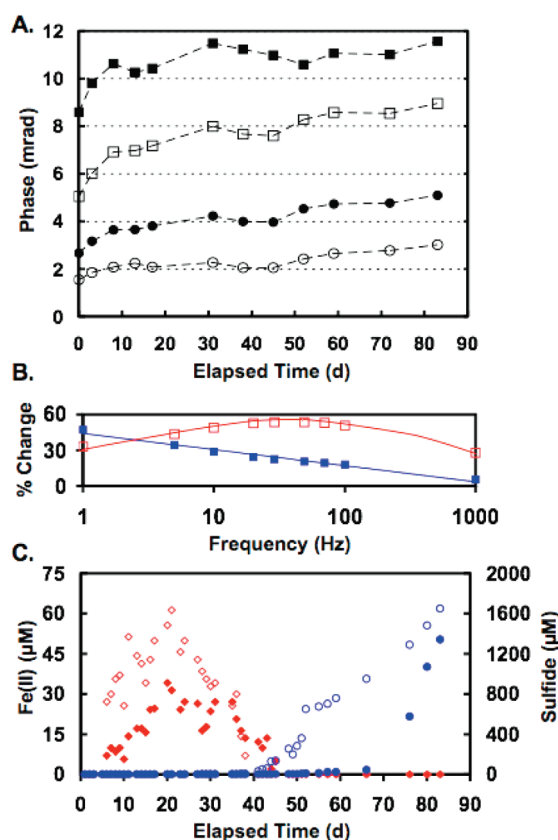

FIGURE 6. Laboratory results. (A) phase response at four frequencies: 1 (○), 10 (●), 100 (□), and 1000 Hz (■). (B) Percent increase in the phase response during iron reduction (red; measured relative to baseline) and sulfate reduction (blue; measured relative to day 45). (C) Fe(II) (red) and dissolved sulfide (blue) concentrations from effluent (filled) and midpoint (open) locations.

During the initial period of Fe(II) accumulation, higher frequencies over the 1−50 Hz range exhibited a larger percentage increase in the phase response relative to baseline than did lower frequencies (Figure 6B); no change as a function of time was observed at frequencies below 1 Hz. Conversely, the relative increase in the phase response following the onset of sulfate reduction (day 45) was greater at low frequency than at high frequency. An excellent inverse correlation between frequency and phase response over the measurement spectrum was observed ($R^2 = 0.97$).

Discussion

Using the IP method, we detected anomalous phase signatures correlated in space and time with stimulated microbial iron and sulfate reduction, with negligible deviation in the phase response in the absence of such activity. The signatures were confined to regions where the accumulation of electroactive ions and the precipitation of sulfide minerals were documented. The spatial development of the phase anomalies was consistent with observations made during a similar IP monitoring experiment the previous year, where the largest increases in the phase response were offset from regions immediately downgradient from the injection boreholes. This was likely the result of preferential flow of acetate within the aquifer (*30*) compounded by alterations in hydrological properties accompanying biomass and precipitate accumulation following carbon amendment (*35*).

The modest increases in resistivity observed in the vicinity of the injection galleries (SI Figure S5) likely tracked the accumulation of mineral precipitates, such as calcite (Figure 5) and FeS, which may exhibit a wide range of size-dependent resistivity values (*11*). Given the small increase in resistivity relative to baseline (<2%), its contribution to the anomalous phase response is inferred to be minor. The elevated phase shift in the baseline images was likely related to reduced geochemical conditions resulting from the injection in the 2005 gallery the previous year, as evidenced by elevated Fe(II) concentrations in M-21, M-22, and M-24 at the time of the baseline data acquisition (Figure 5).

Although we have interpreted the lab and field phase anomalies within the context of an electrode polarization IP mechanism, we cannot completely discount the contribution of other factors in generating the anomalies, such as the growth and accumulation of planktonic and mineral-affixed

biomass during acetate amendment. As noted, other studies (7, 9, 10) have demonstrated the role that cellular components can play in generating IP phase anomalies; however, the magnitude of the phase increase associated with biomass accumulation in these studies has generally been modest (<1−2 mrad). In contrast, studies of the temporal phase behavior accompanying biogenic mineral precipitation (11, 12, 18, 19) have reported phase anomalies more than 1 order of magnitude larger than those involving cells alone. Given the relatively large phase increases reported here (8−12 mrad), it seems most likely that the precipitation of semiconductive minerals and the accumulation of ions capable of facilitating charge transfer reactions are principle underlying factors. Nonetheless, our results highlight the challenges associated with decoupling the myriad contributing factors to anomalous IP responses generated during biostimulation of natural sediments.

Whereas disseminated sulfides resulting from ore-forming (15) and sulfate reducing processes (11, 12) is a well documented source of IP phase anomalies, the generation of anomalies accompanying microbial iron reduction is poorly understood. We propose that the accumulation of Fe(II) in the vicinity of pre-existing mineral phases is capable of enhancing the electrode polarization mechanism contributing to the background IP phase response. Charge transfer across the fluid−mineral interface is enhanced by the presence of Fe(II), which enables the transition in current flow from electrolytic to electronic by lowering the charge transfer resistance across the interface (SI Figure S11). In sediments where iron-reduction is stimulated, the accumulation of Fe(II) could account for an increasing phase response with time.

Even in the absence of an applied electric field, rapid electron transfer from Fe(II) to numerous Fe(III)-bearing mineral phases has been demonstrated (22, 23, 36). During IP measurements, current-induced electron transfer across mineral interfaces can be enhanced as a result of the applied electric field. Under such conditions, the phase offset would be largely controlled by the accumulation of Fe(II) in the vicinity of the mineral grain:

$$\text{Fe(II)} + \text{Fe(III)}_{\text{solid}} \rightarrow \text{Fe(III)} + \text{Fe(II)}_{\text{solid}} \qquad (1)$$
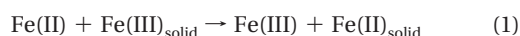
where electrons are passed from Fe(II) to any number of ferric oxide minerals (e.g., hematite, magnetite, and goethite). The reaction is inferred to be largely reversible upon cessation of the applied field or following the change in voltage polarity during IP measurements. Whereas the reduction of the ferric oxide may represent the sole electron transfer pathway (23), the mineral may also act as a conduit for electron transfer from Fe(II) to more oxidized ions sorbed to the mineral surface.

For the results presented here, increasing Fe(II) concentrations likely lowered the charge transfer resistance across the fluid-mineral interface (SI Figure S11; R_{ct}^1), facilitating greater rates of electron transfer and a phase response reflective of a diffusion-controlled process (13, 14, 21). Under such conditions, the composition of the mineral(s) facilitating electron transfer is of minimal importance and in agreement with recently reported results (14) and previous studies investigating the electrochemical nature of the IP response (13).

As a result of mineral precipitation, the phase response during sulfate reduction is inferred to be larger than that occurring during iron reduction. This was documented during both laboratory and field experiments, where the greatest increases in the phase response were observed after the iterative stimulation of both processes and the resultant precipitation of FeS. This created new paths for current flow

primarily dependent upon the presence of dissolved sulfide (S(-II)) (SI Figure S11; R_{ct}^2):

$$\text{S(−II)} + \text{FeS}_{\text{solid}} \rightarrow \text{S}^0 + 2e^- + \text{FeS}_{\text{solid}} \qquad (2)$$
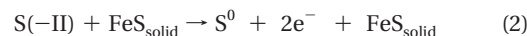
The semiconductive properties of FeS enable electron transfer from dissolved sulfide to more oxidized surface-associated species through the anodic reaction illustrated in eq 2 and consistent with models proposed for similar minerals (37).

Furthermore, modest equilibrium concentrations of Fe(II) (≤6 μM) in the presence of dissolved sulfide and FeS can provide an additional means for facilitating electron transfer during sulfate reduction (38), as shown in eq 3.

$$\text{Fe(II)} + \text{FeS}_{\text{solid}} \rightarrow \text{Fe(III)} + 1e^- + \text{FeS}_{\text{solid}} \qquad (3)$$
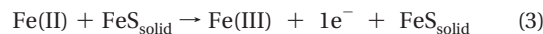
This effect may come to dominate when Fe(II) and FeS are present, as was the case during IP measurements made on day 57, or when poststimulation conditions favor Fe(II) rather than S(−II) as the dominant electroactive species.

The observed frequency-dependent IP response may also result from rapid electron transfer by sorbed versus aqueous electroactive ions. Under the pH conditions of the laboratory and field experiments, a large fraction of the Fe(II) formed during iron reduction sorbs to iron oxide surfaces (39). As a result, charge transfer across the fluid−mineral interface is expected to occur even during the high frequency measurements due to the minimal time required for diffusion to and adsorption onto the mineral surface (21). Whereas the Fe(II)-dependent high frequency phase response was documented in the laboratory experiment, we can only rely upon the 1 Hz data to support the proposed IP mechanism under field conditions. Where possible, efforts to correct subsequent field high frequency measurements for electromagnetic artifacts are warranted, as the laboratory experiment indicated greater sensitivity to the accumulation of Fe(II) at frequencies approaching 100 Hz. Until scaling issues are addressed, however, direct comparisons between laboratory and field measurements at a given frequency must be considered qualitative.

The enhanced sensitivity of the low frequency measurements to aqueous sulfide and metal sulfides is interpreted to result from the longer time scales involved in sulfide-mediated faradaic processes. Diffusion of sulfide and sorption onto mineral surfaces are required in advance of charge transfer across the fluid−mineral interface. Although data is sparse, sulfide-mediated electron transfer reactions appear to proceed more slowly than those involving Fe(II) (26), possibly due to the slower two-electron transfer indicated in eq 2. The more sluggish charge transfer kinetics should theoretically lead to larger phase anomalies at lower frequency, where applied voltages are maintained for extended periods of time.

Our results represent the first field demonstration of an IP monitoring approach designed to track geochemical and mineralogical changes accompanying stimulated subsurface bioremediation. The approach may be generally applicable to spatially extend geochemical data from a limited number of boreholes providing valuable information for assessing remediation efficacy over large spatial scales. We report a frequency-dependent phase response sensitive to both the predominant metabolic process (i.e., iron or sulfate reduction) and the accumulation of biogenic mineral precipitates (e.g., FeS). The spectral effect was corroborated using a laboratory column experiment where stimulation of the two metabolic pathways was sufficiently offset in time to allow for evaluation of their independent contributions to the IP response. While different forms of charge transfer accompanying iron and sulfate reduction are believed to be responsible for the spectral effect, investigation of other

frequency dependent IP mechanisms, such as biofilm formation, mineral growth, and aging, and the precipitation of secondary minerals (e.g., calcite), is warranted.

Supporting Information Available

Additional field and laboratory IP data, TEM micrographs of cell-mineral aggregates, and a schematic representation of pore scale charge transfer pathways. This material is available free of charge via the Internet at http://pubs.acs.org.

Literature Cited

(1) Barkay, T.; Schaefer, J. Metal and radionuclide bioremediation: Issues, considerations and potentials. *Curr. Opin. Microbiol.* **2001**, *4* (3), 318–323.

(2) Anderson, R. T.; Vrionis, H. A.; Ortiz-Bernad, I.; Resch, C. T.; Long, P. E.; Dayvault, R.; Karp, K.; Marutzky, S.; Metzler, D. R.; Peacock, A.; White, D. C.; Lowe, M.; Lovley, D. R. Stimulating the in situ activity of Geobacter species to remove uranium from the groundwater of a uranium-contaminated aquifer. *Appl. Environ. Microbiol.* **2003**, *69* (10), 5884–5891.

(3) Wu, W. M.; Carley, J.; Gentry, T.; Ginder-Vogel, M. A.; Fienen, M.; Mehlhorn, T.; Yan, H.; Caroll, S.; Pace, M. N.; Nyman, J.; Luo, J.; Gentile, M. E.; Fields, M. W.; Hickey, R. F.; Gu, B. H.; Watson, D.; Cirpka, O. A.; Zhou, J. Z.; Fendorf, S.; Kitanidis, P. K.; Jardine, P. M.; Criddle, C. S. Pilot-scale in situ bioremediation of uranium in a highly contaminated aquifer. 2. Reduction of U(VI) and geochemical control of U(VI) bioavailability. *Environ. Sci. Technol.* **2006**, *40* (12), 3986–3995.

(4) Rubin, Y.; Hubbard, S. S. Hydrogeophysics; 1st ed.; Springer: Netherlands, 2005; *50*, p 523.

(5) Abdel Aal, G. Z.; Atekwana, E. A.; Slater, L. D.; Atekwana, E. A. Effects of microbial processes on electrolytic and interfacial electrical properties of unconsolidated sediments. *Geophys. Res. Lett.* **2004**, *31* (12), L12505.

(6) Allen, J. P.; Atekwana, E. A.; Atekwana, E. A.; Duris, J. W.; Werkema, D. D.; Rossbach, S. The microbial community structure in petroleum-contaminated sediments corresponds to geophysical signatures. *Appl. Environ. Microbiol.* **2007**, *73* (9), 2860–2870.

(7) Ntarlagiannis, D.; Yee, N.; Slater, L. On the low-frequency electrical polarization of bacterial cells in sands. *Geophys. Res. Lett.* **2005**, *32* (24), L24402.

(8) Williams, K. H.; Hubbard, S. S.; Banfield, J. F. Galvanic interpretation of self-potential signals associated with microbial sulfate-reduction. *J. Geophys. Res.* **2007**, *112*, G03019.

(9) Abdel Aal, G. Z.; Atekwana, E.; Radzikowski, S.; Rossbach, S. Effect of bacterial adsorption on low frequency electrical properties of clean quartz sands and iron-oxide coated sands. *Geophys. Res. Lett.* **2009**, *36*, L04403.

(10) Davis, C. A.; Atekwana, E.; Atekwana, E.; Slater, L. D.; Rossbach, S.; Mormile, M. R. Microbial growth and biofilm formation in geologic media is detected with complex conductivity measurements. *Geophys. Res. Lett.* **2006**, *33* (18), L18403.

(11) Williams, K. H.; Ntarlagiannis, D.; Slater, L. D.; Dohnalkova, A.; Hubbard, S. S.; Banfield, J. F. Geophysical imaging of stimulated microbial biomineralization. *Environ. Sci. Technol.* **2005**, *39* (19), 7592–7600.

(12) Ntarlagiannis, D.; Williams, K. H.; Slater, L. D.; Hubbard, S. S. Low frequency electrical response to microbial induced sulfide precipitation. *J. Geophys. Res.* **2005**, *110*, G02009.

(13) Angoran, Y.; Madden, T. R. Induced polarization: A preliminary study of its chemical basis. *Geophysics* **1977**, *42* (4), 788–803.

(14) Merriam, J. B. Induced polarization and surface electrochemistry. *Geophysics* **2007**, *72* (4), F157–F166.

(15) Pelton, W. H.; Ward, S. H.; Hallof, P. G.; Sill, W. R.; Nelson, P. H. Mineral discrimination and removal of inductive coupling with multifrequency-IP. *Geophysics* **1978**, *43* (3), 588–609.

(16) Slater, L. D.; Glaser, D. R. Controls on induced polarization in sandy unconsolidated sediments and application to aquifer characterization. *Geophysics* **2003**, *68* (5), 1547–1558.

(17) Vinegar, H. J.; Waxman, M. H. Induced polarization of shaly sands. *Geophysics* **1984**, *49* (8), 1267–1287.

(18) Personna, Y. R.; Ntarlagiannis, D.; Slater, L.; Yee, N.; O'Brien, M.; Hubbard, S. Spectral induced polarization and electrodic potential monitoring of microbially mediated iron sulfide transformations. *J. Geophys. Res.* **2008**, *113*, G02020.

(19) Slater, L.; Ntarlagiannis, D.; Personna, Y. R.; Hubbard, S. Pore-scale spectral induced polarization signatures associated with FeS biomineral transformations. *Geophys. Res. Lett.* **2007**, *34* (21), L21404.

(20) Marcus, R. A. Theory of electron-transfer reaction rates of solvated electrons. *J. Chem. Phys.* **1965**, *43* (10P1), 3477–3495.

(21) Bard, A. J.; Faulkner, L. R., *Electrochemcial Methods: Fundamentals and Applications*; John Wiley & Sons, Inc.: 2001.

(22) Iordanova, N.; Dupuis, M.; Rosso, K. M. Charge transport in metal oxides: A theoretical study of hematite alpha-Fe_2O_3. *J. Chem. Phys.* **2005**, *122* (14), 144305.

(23) Williams, A. G. B.; Scherer, M. M. Spectroscopic evidence for Fe(II)-Fe(III) electron transfer at the iron oxide-water interface. *Environ. Sci. Technol.* **2004**, *38* (18), 4782–4790.

(24) Gehin, A.; Greneche, J. M.; Tournassat, C.; Brendle, J.; Rancourt, D. G.; Charlet, L. Reversible surface-sorption-induced electron-transfer oxidation of Fe(II) at reactive sites on a synthetic clay mineral. *Geochim. Cosmochim. Acta* **2007**, *71* (4), 863–876.

(25) Kozerski, G. E.; Fiorentino, M. A.; Ketterer, M. E. Determination of aqueous Fe III/II electron self-exchange rates using enriched stable isotope labels, ion chromatography, and inductively coupled plasma mass spectrometry. *Anal. Chem.* **1997**, *69* (4), 783–788.

(26) Sun, J. F.; Stanbury, D. M. Trace metal-ion catalysis of oxidation of aqueous hydrogen sulfide by outer-sphere oxidants. *Inorg. Chim. Acta* **2002**, *336*, 39–45.

(27) Ateya, B. G.; Al Kharafi, F. M.; Alazab, A. S. Kinetics of the electrochemical oxidation of sulfide ions. *Abstr. Pap. Am. Chem. Soc.* **2004**, *228*, U852–U852.

(28) Slater, L.; Ntarlagiannis, D.; Wishart, D. On the relationship between induced polarization and surface area in metal-sand and clay-sand mixtures. *Geophysics* **2006**, *71* (2), A1–A5.

(29) Wong, J. An electrochemical model of the induced-polarization phenomenon in disseminated sulfide ores. *Geophysics* **1979**, *44* (7), 1245–1265.

(30) Vrionis, H. A.; Anderson, R. T.; Ortiz-Bernad, I.; O'Neill, K. R.; Resch, C. T.; Peacock, A. D.; Dayvault, R.; White, D. C.; Long, P. E.; Lovley, D. R. Microbiological and geochemical heterogeneity in an in situ uranium bioremediation field site. *Appl. Environ. Microbiol.* **2005**, *71* (10), 6308–6318.

(31) Cline, J. D. Spectrophotometric determination of hydrogen sulfide in natural waters. *Limnol. Oceanogr.* **1969**, *14* (3), 454–458.

(32) Lovley, D. R.; Phillips, E. J. P. Rapid assay for microbially reducible ferric iron in aquatic sediments. *Appl. Environ. Microbiol.* **1987**, *53* (7), 1536–1540.

(33) Kemna, A.; Binley, A.; Slater, L. Crosshole IP imaging for engineering and environmental applications. *Geophysics* **2004**, *69* (1), 97–107.

(34) Kemna, A.; Binley, A.; Ramirez, A.; Daily, W. Complex resistivity tomography for environmental applications. *Chem. Eng. J.* **2000**, *77*, 11–18.

(35) Li, L.; Steefel, C. I.; Williams, K. H.; Wilkins, M. J.; Hubbard, S. S. Mineral transformation and biomass accumulation associated with uranium bioremediation at Rifle, colorado. *Environ. Sci. Technol.* **2009**, *43* (14), 5429–5435.

(36) Rosso, K. M.; Dupuis, M. On charge transport in iron oxides. *Geochim. Cosmochim. Acta* **2005**, *69* (10), A778–A778.

(37) Becker, U.; Rosso, K. M.; Hochella, M. F. The proximity effect on semiconducting mineral surfaces: A new aspect of mineral surface reactivity and surface complexation theory. *Geochim. Cosmochim. Acta* **2001**, *65* (16), 2641–2649.

(38) Burton, E. D.; Bush, R. T.; Sullivan, L. A.; Mitchell, D. R. G. Reductive transformation of iron and sulfur in schwertmannite-rich accumulations associated with acidified coastal lowlands. *Geochim. Cosmochim. Acta* **2007**, *71* (18), 4456–4473.

(39) Roden, E. E.; Urrutia, M. M., III. **2002**, *19* (2), 209–251.